

# EUROPEAN SYNCHROTRON RADIATION FACILITY

## Experimental Report MD-711: Carole Poitry-Yamate

Neuron-glia interactions in mammalian brain combining non-invasive  $^{18}\text{F}$ FDG PET and HEXRF imaging

In contrast to imaging  $^{18}\text{F}$ FDG-6P at millimeter length scales using  $^{18}\text{F}$ FDG PET, synchrotron-based x-ray fluorescence spectromicroscopy (XRF) (Westneat et al. 2008) allows imaging the structurally identical molecule, albeit non-radiolabeled, at subcellular spatial resolution. We recently demonstrated the feasibility of direct mapping in brain of  $^{19}\text{F}$  in FDG-6P using soft (low-energy) x-ray fluorescence (LEXRF) *in vitro* and *in vivo* for cerebral and retinal glia (Poitry-Yamate et al. 2013a). Those results were later extended to show that cerebral neurons also transport and phosphorylate  $^{19}\text{F}$ FDG (Poitry-Yamate et al. 2013b), an indication that both glial cells and neurons are glycolytically active. In proposal MD-711, we sought *in vivo* evidence for the cellular locus of IAA uptake by imaging the distribution of iodine in IAA over cortical brain regions using hard (high-energy) x-ray fluorescence (HEXRF). In spite of its extended use since the 1930's (Webb 1966), IAA has hitherto not been imaged by any modality in the literature. This prompted us to first perform a proof of concept IAA HEXRF experiment in the visual system, i.e. retina of the CNS where the effect of IAA on structure, function and metabolism has been exceptionally documented at great length, e.g. (Noell 1951). The rationale linking IAA and FDG-6P imaging and CMRglc follows from our working hypothesis that brain cells metabolizing endogenous glucose-6P down the glycolytic pathway during  $^{18}\text{F}$ FDG PET imaging are directly sensitive to the effects of IAA. Gadolinium measurements were also performed on brain tissue, and served as control samples within the context of the present project.

Iodoacetate (IAA), a compound of choice to inhibit the metabolism of glucose through glycolysis to pyruvate/lactate, was administered systemically in rats to evaluate its effect on brain glucose utilization and its cellular target of uptake. Co-administration of iodoacetate (40mg/kg) and [ $^{18}\text{F}$ ]-2-deoxy-2-fluoro-D-glucose ( $^{18}\text{F}$ FDG, ~50MBq) under euglycemic conditions reduced the mean rate of resting cerebral glucose utilization (CMRglc), from  $50.1 \pm 0.3$  to  $23.6 \pm 0.3$   $\mu\text{mol}/100\text{g}/\text{min}$ . Time-activity curves showed that  $^{18}\text{F}$ FDG extraction by the brain was reduced by IAA, while Patlak graphical analysis and 3-compartment modeling showed that this reduced extraction was linked to a reduction of phosphorylated  $^{18}\text{F}$ FDG per unit time, and not to glucose transport. IAA's concentration-dependent effect on intracellular metabolism was temporally linked to secondary increases of  $^{18}\text{F}$ FDG in plasma, and hyperglycemia at 50 min post-injection, at which time imaged  $^{18}\text{F}$ FDG-6P fell from  $2.57 \pm 0.26$  g/ml to  $1.97 \pm 0.21$  g/ml. These results suggest that IAA's inhibitory effect, at concentrations that block retinal glycolysis *in vivo*, limited cerebral ATP availability for the hexokinase reaction. Under these neuroglycopenic conditions, synchrotron-based hard x-ray fluorescence mapping of cortical IAA at <1 micron spatial resolution was performed. Surprisingly, IAA was disproportionately high in cortical pyramidal neurons and interneurons, and its subcellular distribution mirrored that of  $^{19}\text{F}$ FDG-6-phosphate (Poitry-Yamate et al. 2013b). These results indicate that glycolytically active brain cells are directly sensitive to the effects of IAA, and they lend support for a glycolytic capacity of neurons *in vivo*. We concluded that both neurons and astrocytes contribute to the non-invasive  $^{18}\text{F}$ FDG PET signal.

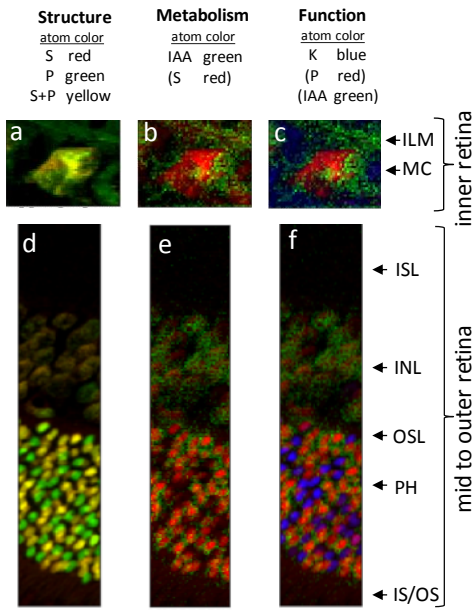


**Fig. 1 Validation of HEXRF imaging of IAA *in vivo* at  $1\mu\text{m}^2$  resolution.** (a) HEXRF maps of P and S of the inner retina, highlighting the structure of the Müller glial cell endfoot (MC), part of which forms the inner limiting membrane (ILM). (b) spatial distribution of IAA (green) in the region shown in a, using the S map (in red) as reference. (c) spatial distribution of potassium (K, in blue) in the region shown in a, using the P (in red) and IAA (in green) maps as reference. (d) same as in a, but from the mid to outer retina. (e) same as in b, but from the mid to outer retina. (f) same as in c, but from the mid to outer retina. ISL, inner synaptic layer; INL, inner nuclear layer; OSL, outer synaptic layer; PH, layer containing photoreceptor cell soma; IS/OS, inner and outer photoreceptor segments. Scale bar:  $20\mu\text{m}$ .

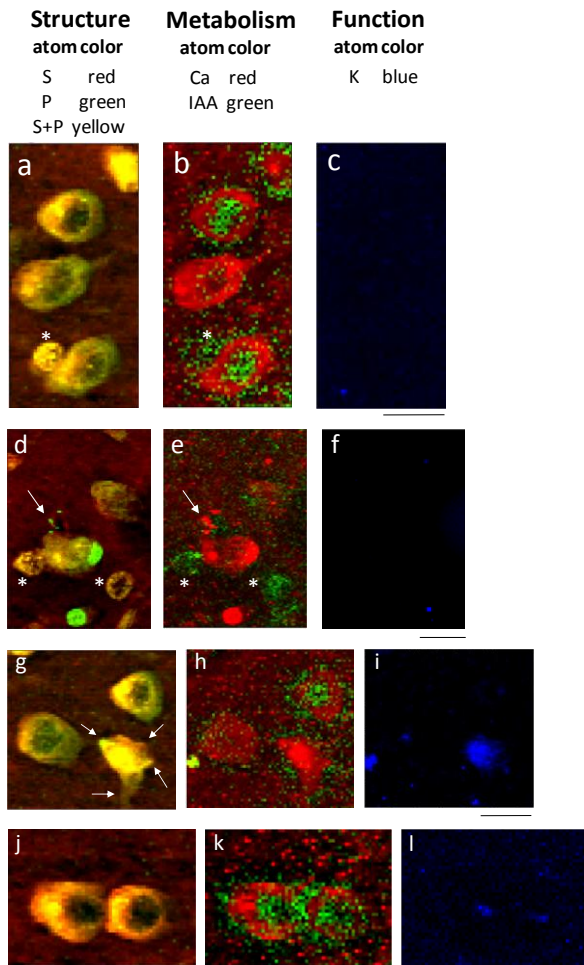


**Fig. 2 Subcellular distribution of IAA in cortical neurons imaged at  $1\mu\text{m}^2$  resolution *in situ*.** (a) cytoarchitecture of cortical layer V pyramidal neurons and interneurons, using HEXRF mapping of P (green) and S (red). (b) subcellular distribution of IAA (in green) of the region shown in a, using the Ca map as reference. Interneurons are identified by the asterisks. (c) cellular distribution of K in the region shown in a. (d-f) analogous to a-c, but from a different region of cortical layer III-V. Arrows point to neuron processes. (g-i) analogous to a-c, but from a different region of cortical layer III-V. Arrows point to multiple processes arising from the soma of a putative astrocyte. (j-l) analogous to a-c, but from a different region of cortical layer III-V. Scale bar:  $20\mu\text{m}$ .